# Vacancies and vacancy-oxygen complexes in silicon: Positron annihilation with core electrons

J. Kuriplach*

*Department of Subatomic and Radiation Physics, University of Ghent, Proeftuinstraat 86, B-9000 Ghent, Belgium
and Department of Low Temperature Physics, Charles University, V Holešovičkách 2, CZ-180 00 Prague 8, Czech Republic*

A. L. Morales

*Department of Physics, University of Antioquia, A.A. 1226, Medellín, Colombia*

C. Dauwe and D. Segers

*Department of Subatomic and Radiation Physics, University of Ghent, Proeftuinstraat 86, B-9000 Ghent, Belgium*

M. Šob

*Institute of Physics of Materials, Academy of Sciences of the Czech Republic, Žižkova 22, CZ-616 62 Brno, Czech Republic*

(Received 16 October 1997)

Various point defects in silicon are studied theoretically from the point view of positron annihilation spectroscopy. Properties of a positron trapped at a single vacancy, divacancy, vacancy-oxygen complexes ($VO_n$), and divacancy-oxygen complex are investigated. In addition to the positron lifetime and positron binding energy to defects, we also calculate the momentum distribution of annihilation photons (MDAP) for high momenta, which has been recently shown to be a useful quantity for defect identification in semiconductors. The influence of atomic relaxations around defects on positron properties is also examined. Mutual differences among the high momentum parts of the MDAP for various defects studied are mostly considerable, which can be used for the experimental defect determination. [S0163-1829(98)03039-2]

## I. INTRODUCTION

Silicon is nowadays widely used for the fabrication of electronic devices. Their electrical behavior can be significantly affected by vacancylike defects existing in the material as these defects can introduce energy levels in the band gap in addition to energy levels introduced by doping. Numerous types of point defects have been found and studied in Si. Their role is not yet fully understood and their further investigation is, therefore, highly desirable.

Si crystals are usually produced by the Czochralski (Cz) growth process or float-zone (FZ) technique. In the former crystals oxygen atoms exist in a higher amount and a typical concentration is about $10^{18}\,cm^{-3}$, whereas the oxygen content in FZ Si is typically two orders of magnitude lower. Due to a relatively high concentration of oxygen in Cz Si, oxygen-related defects in Si have attracted appreciable attention.[1]

If Si crystals are irradiated by electrons at room temperature, vacancies, divacancies (or clusters of vacancies), and Si interstitials are created.[2,3] The single vacancy $V$ is not stable at room temperature and either recombines, forms the $VO$ defect (i.e., vacancy-oxygen complex or $A$ center) by capturing an interstitial oxygen atom, $O_i$, or joins further vacancies to create vacancy aggregates. A further annealing of samples with $VO$ defects causes (among other processes) a $VO \rightarrow VO_2$ transition and probably $VO_2 \rightarrow VO_3$ at higher temperatures.[4,5] Concerning the divacancy, $V_2$, Trauwaert *et al.*[6] have recently found that this defect is probably transformed into the divacancy-oxygen complex ($V_2O$) upon a low-temperature anneal. Due to indirect experimental evidence[6] a further verification of the existence of the $V_2O$ complex is needed. The kinetics of processes mentioned above depend on the oxygen concentration and can thus be substantially different in Cz and FZ silicon samples.

Positron annihilation spectroscopy is a well-established tool to probe defects in solids.[7] This technique is especially convenient for vacancies and vacancy-related defects as they act as positron traps. We should mention, however, that positron lifetime spectroscopy (PLS), often used for defect studies, fails to distinguish among positron traps if there are several ones with similar characteristic positron lifetimes. On the other hand, even if these defects have similar lifetimes, the momentum distribution of annihilation photons (MDAP) can differ significantly. Namely, the MDAP for small values of momenta corresponds mainly to positron annihilation with valence electrons. On the contrary, annihilation with core electrons results in a much broader momentum distribution. The configuration of core electrons is characteristic for each atom and in this way distinct defects may be identified as they have different atomic environments. This is the basic idea of the paper published recently by Alatalo *et al.*[8] In this work the InP system is taken as an example and the difference of the high momentum regions of the Doppler broadened annihilation line is clearly seen for In and P vacancies. A theoretical model for calculations of the high momentum parts (HMP's) of the MDAP is also presented in Ref. 8. This model has been further developed[9] and a very good quantitative agreement with experiment has been achieved (with the exception of transition metals; see also Ref. 10).

Let us note, however, that HMP's, as considered in this work, are not identical with so-called high momentum components (HMC's) of the MDAP originating from valence electrons. Such HMC's arise due to the presence of images

of the electron bands within the central Brillouin zone in the extended zone scheme.[11] The HMC's are usually assumed to decrease very strongly with increasing momentum (see also below). In the following our HMP's mean solely the core electron contribution to the MDAP.

To our knowledge there have been a few experimental works[12–16] where the technique of HMP measurement has been applied to Si. As there was no theoretical study examining the HMP behavior for defects in Si (partially except Ref. 17 published recently), we decided to perform such calculations for some of the frequently studied defects to allow for an interpretation of experimental data. In our previous paper[18] we have presented results of calculations based on the atomic superposition[19] (ATSUP) method and we have determined the positron lifetimes and HMP's of the MDAP for a few types of vacancylike defects in Si. Namely, we have studied $V$, $V_2$, $VO_n$ ($n = 1$, 2, and 3), and $V_2O$ defects. The differences found in calculated HMP curves indicate that the defects could be experimentally well distinguishable. We have also shown preliminary HMP measurements carried out on irradiated and defect-free Cz and FZ Si samples. Here we substantially extend this study giving important computational details not specified in Ref. 18 and employing also a self-consistent *ab initio* technique. Moreover, we compare positron properties obtained within two different approaches to the electron-positron correlations.

Relaxations of atoms surrounding a defect in semiconductors represent a very important point. For instance, an inward relaxation around a vacancy decreases the free volume to trap positrons. Consequently, the positron lifetime decreases and the HMP's increase as the overlap of positron wave function with nearest atoms (core states) also increases. But if one considers that a positron is trapped in this defect, relaxations change[20–22] due to the electrostatic interaction of the trapped positron with neighboring atoms (ions). The positron characteristics then change too. In our calculations we consider the first type of relaxation only, i.e., relaxations caused by the introduction of a defect itself. We do not compute them, but take known relaxations from the literature (see Sec. II A). Furthermore, we restrict ourselves to the neutral charge states of defects considered.

The paper is organized as follows. In Sec. II we explain our theoretical approach, especially how the electron and positron states in the systems studied are determined (Sec. II A) and the way of HMP calculations (Sec. II B). Results are presented and discussed in Sec. III. The paper is concluded in Sec. IV.

## II. COMPUTATIONAL METHOD

### A. Positron states and electron structure

In the following we adopt the so-called zero positron density limit[23,24] to study positron properties in solids. Within this limit a positron feels the potential that is a sum of two parts. The first part is the Coulomb potential produced by the charge distribution of surrounding electrons and nuclei while the second part originates from the electron-positron correlations. The electron potential is considered not to be influenced by the presence of positrons. The positron potential specified above depends only on the electron density (and on positions and charges of nuclei, of course).

To obtain the electron density needed for the construction of the positron potential, we have chosen two distinct theoretical approaches. First is the atomic superposition method,[19] which makes use of electron densities of free atoms to construct the electron density of the whole crystal. Second, we employ the linear muffin-tin orbital (LMTO) method within the atomic-sphere approximation[25] (ASA) so that we can determine the electron distribution self-consistently. Another difference between these two methods is that the ATSUP one does not impose any shape restriction for the positron potential and density in contrast to the LMTO ASA, within which the density and potential are spherically averaged (for both positrons and electrons).

The Coulomb potential for positrons is just the Coulomb potential for electrons with the opposite sign and one can take the electron Coulomb potential obtained from the computation of the electron structure of the system studied. For the correlation part we use the parametrization of Arponen and Pajanne's[26] results given by Boroński and Nieminen (BN).[27] Due to the incomplete screening of positrons in semiconductors, a correction[28] (based on the notion of screening in dielectric materials) has to be applied; we will further refer to this case as to BN calculations or scheme (see also Sec. II B). For comparison, we also apply the formula recently introduced by Barbiellini *et al.*[29] based on the generalized gradient approximation (GGA) for electron-positron correlations (referred to in the following as GGA calculations or scheme). Once the positron potential is known, a Schrödinger-like equation[23,24] is solved to find the positron ground state and energy.

A significant theoretical effort has been devoted to the determination of various properties of points defects in Si. The single vacancy and divacancy in the neutral charge state belong to the simplest defects and their electron structure and geometry have been thoroughly studied.[22,30–34] In our calculations we use the atomic positions of relaxed $V$ and $V_2$ defects taken from the geometry relaxation performed by Seong and Lewis[33] who have utilized a pseudopotential approach together with the supercell technique. In the present work we take into account only the relaxations of the first nearest neighbors of the single vacancy and divacancy. The vacancy-oxygen complexes have been studied theoretically by Chadi[30] and very recently by Ewels *et al.*[5] In the latter work hydrogen-terminated clusters are relaxed using a conjugate-gradient method. Our study of $VO_n$ ($n = 1$, 2, and 3) and $V_2O$ complexes is based on relaxed geometries determined in Ref. 5.

In our calculations, we utilize the supercell approach to model point defects and choose the lattice constant of Si to be 10.2768 a.u.[35] It is desirable that the supercells are as large as possible to avoid interactions among defects. In the case of the ATSUP method, we use supercells based on the 216-atom supercell of perfect Si, whereas 64-atom-based supercells are used with the LMTO method as this technique is substantially more demanding than the ATSUP one. To obtain the supercell corresponding to a defect, we remove Si atom(s) [and add O atom(s)]; eventually atoms are moved to the relaxed positions. Concerning the LMTO calculations, we include $s$, $p$, and $d$ states into the basis (with $d$ states treated as downfolded[25]). The same basis is considered for positrons and an iterative scheme for finding the pivotal en-

ergy parameters ($E_\nu$'s) is employed.[36] Empty spheres have to be included into the supercell to describe properly the charge distribution in open structures like diamond.

To examine the adequacy of our method of self-consistent electron structure calculations, we studied the density of states (DOS) for ideal and relaxed $V_2$ defects (with 16-atom-based supercells only). The DOS curves obtained have features similar to those found in Refs. 32 and 33. However, the positions of particular energy levels, which correspond to defects, differ. This demonstrates the sensitivity of electron structure studies of defects in semiconductors to computational techniques employed.[33]

### B. Momentum distribution

The approach used here to calculate the HMP's of the MDAP is based on the notion of the state-dependent enhancement factor. The idea of state-dependent enhancement was introduced by Šob[37,38] for valence electrons in $d$ metals and their intermetallic compounds. It was used subsequently for the analysis of the positron annihilation spectra in various metallic systems containing $d$ electrons.[39–43] Average core enhancement factors were found in Refs. 44 and 45 and their momentum dependence was discussed by Daniuk *et al.*[46,47] Recently, it has been shown that the concept of state-dependent enhancement factor can be justified by applying the Jastrow approximation[48] to the problem of the correlations of an electron-positron pair (see Refs. 9 and 49 for a detailed discussion).

Thus, the contribution $\rho^i(\mathbf{p})$ to the MDAP of an electron state $j$ described by the wave function $\psi_-^j$ reads

$$\rho^j(\mathbf{p}) = \pi r_e^2 c \gamma^j \left| \int \exp(-i\mathbf{p}\cdot\mathbf{r}) \psi_-^j(\mathbf{r}) \psi_+(\mathbf{r}) d\mathbf{r} \right|^2, \quad (1)$$

where $r_e$ is the classical radius of electron, $c$ is the speed of light, $\gamma^j$ stands for the enhancement factor of the state $j$, and $\psi_+$ denotes the positron wave function.

In the case of annihilation with core electrons, Eq. (1) can be simplified considerably. In principle, all core states of all atoms in the system contribute to the HMP's of the MDAP and the contribution from the $i$th atom and a shell characterized by principal ($n$) and orbital ($l$) quantum numbers is given by the following formula[9]

$$\rho^{i,nl}(p) = 4\pi^2 r_e^2 c N^{i,nl} \gamma^{i,nl} \left| \int R_+^i(r) R_-^{i,nl}(r) j_l(pr) r^2 dr \right|^2. \quad (2)$$

In this equation $N^{i,nl}$ denotes the number of electrons in the ($n,l$) shell, $j_l$ is the spherical Bessel function, and $R_-^{i,nl}$ and $R_+^i$ are, respectively, electron and positron radial wave functions. We suppose that the positron wave function is predominantly of $s$ character. The enhancement factor $\gamma^{i,nl}$ is equal to the ratio $\lambda_{enh}^{i,nl}/\lambda_{IPM}^{i,nl}$, where $\lambda^{i,nl}$ stands for the partial annihilation rate corresponding to the ($n,l$) core state of the $i$th atom determined using the expression

$$\lambda^{i,nl} = \pi r_e^2 c \int |\psi_+(\mathbf{r})|^2 n_-^{i,nl}(|\mathbf{r}-\mathbf{r}_i|) \gamma[n_-(\mathbf{r})] d\mathbf{r}. \quad (3)$$

Here $n_-^{i,nl}$ denotes the (per one electron) radial core electron density of the ($n,l$) orbitals of the $i$th atom (placed at $\mathbf{r}_i$

position) and $\gamma$ is a "standard" electron enhancement factor describing the pileup of electrons at the positron site.[23,24] The subscript IPM in the $\gamma^{i,nl}$ ratio means that the corresponding partial annihilation rate was calculated within the independent particle model[23] (IPM), i.e., $\gamma = 1$, whereas $\lambda_{enh}$ is calculated using either Boroński-Nieminen[27,28] or generalized gradient approximation[29] enhancement factor. The dielectric constant enters the expression[28] for $\gamma_{BN}$ and we use the value $\epsilon = 12$. In the case of GGA the adjustable parameter $\alpha = 0.22$ (Ref. 29) is applied. The same values of $\epsilon$ and $\alpha$ are taken into account when calculating the positron correlation potential (see Sec. II A).

The resulting HMP's of the MDAP corresponding to the one-dimensional momentum distribution, measured, e.g., by Doppler broadening spectroscopy of the annihilation line, are then given by the sum over all atomic sites and corresponding core shells[9]

$$\rho(p) = \sum_{i,nl} \int_p^\infty \rho^{i,nl}(p') p' dp'. \quad (4)$$

We recall again that the above formula applies for annihilation with core electrons only. In the work of Hakala, Puska, and Nieminen[17] both valence and core electron contributions to the MDAP are given for the bulk Si. On the basis of this paper one can conclude that the comparison of calculated and measured dependencies is meaningful for momenta $p \gtrsim 15 \times 10^{-3} m_e c$. In the following we use preferably mrad units for momentum; $1 \times 10^{-3} m_e c$ corresponds to 1 mrad deviation from the antiparallel directions of annihilation $\gamma$ rays (and to a Doppler shift of 0.26 keV).

A few points concerning numerics require a discussion. First, to obtain $R_+^i(r)$ functions within the ATSUP scheme, a 64-point 3D-interpolation function[50] on the 3D mesh is used. Furthermore, a $R_+^i(r)$ function is not unambiguous and depends on the direction chosen for expansion. We have found small differences among HMP results obtained using expansions in different directions and we have decided to make rather a spherical average of the positron wave function.

Second, we have not put any explicit upper limit in the integral in Eq. (2). Its choice depends on the system considered (i.e., extension of outermost core shells). In the case of Si (and O) we have found that 5 a.u. is already enough to get results that do not change when this parameter is increased. Oscillations that could appear when the integration is cut at a short distance from nuclei do not appear. Our way of calculating the integral in Eq. (2) differs from that used in Ref. 9 in one respect. Namely, we prefer to use the positron wave function determined for the system under consideration instead of using a model function with several parameters found by a fitting procedure applied to the wave function determined for the corresponding monoatomic system (see Ref. 9 for details). In the case of the LMTO method, we keep the positron radial wave function at the value $R_+^i(w_i)$ for $r > w_i$, where $w_i$ is the radius of the $i$th atomic sphere. Empty spheres are assumed not to contribute to the HMP's of the MDAP.

Third, the radial core electron densities, $n_-^{i,nl}$'s, are calculated by the well-known Desclaux's atomic code[51] and used both in ATSUP and LMTO schemes. This makes the comparison of the HMP results obtained with these two tech-

TABLE I. Positron lifetimes ($\tau$), core annihilation rates ($\lambda_c$), and binding energies ($E_b$) calculated using the ATSUP method. Experimental lifetimes ($\tau_{expt}$) taken from the work of Saito and Oshiyama (Ref. 22) are also shown. Numbers in parentheses in the column $\lambda_c$ give the relative core annihilation rate (in %) with respect to the total rate. Both BN and GGA schemes have been used.

| System | ATSUP-BN | | | ATSUP-GGA | | | |
| | $\tau$ (ps) | $\lambda_c$ (ns$^{-1}$) (%) | $E_b$ (eV) | $\tau$ (ps) | $\lambda_c$ (ns$^{-1}$) (%) | $E_b$ (eV) | $\tau_{expt}$ (ps) |
|---|---|---|---|---|---|---|---|
| Bulk | 218 | 0.143 (3.1) | | 208 | 0.093 (1.9) | | 218 |
| $V$ ideal | 252 | 0.095 (2.4) | 0.36 | 242 | 0.063 (1.5) | 0.32 | |
| $V$ relaxed | 225 | 0.137 (3.1) | +0.00 | 215 | 0.089 (1.9) | $-0.01$ | 270 |
| $VO$ relaxed | 225 | 0.175 (3.9) | 0.06 | 217 | 0.108 (2.3) | 0.01 | |
| $VO_2$ relaxed | 222 | 0.231 (5.1) | 0.10 | 218 | 0.126 (2.7) | 0.01 | |
| $VO_3$ relaxed | 218 | 0.220 (4.8) | 0.03 | 214 | 0.120 (2.6) | $-0.05$ | |
| $V_2$ ideal | 302 | 0.052 (1.6) | 1.22 | 302 | 0.035 (1.1) | 1.09 | |
| $V_2$ relaxed | 286 | 0.064 (1.8) | 0.93 | 280 | 0.043 (1.2) | 0.83 | 295–325 |
| $V_2O$ relaxed | 297 | 0.106 (3.1) | 1.24 | 304 | 0.067 (2.0) | 1.05 | |

niques more explicit. An $R_-^{i,nl}$ function is taken to be the square root of the corresponding radial density ($n_-^{i,nl}$).

Fourth, even if one uses a quite large number of grid points in the 3D mesh within the ATSUP method, there appear oscillations of the $\rho(p)$ function for a given $p$ with respect to the number of mesh points. In the HMP results shown below we use the average of results obtained using $97^3$ (i.e., $97 \times 97 \times 97$), $98^3$, $99^3$, and $100^3$ mesh points, which attenuates the oscillations mentioned considerably. In general, the positron wave function needs to be determined very accurately in the region close to nuclei, in contrast to lifetime calculations where this region is not so important. Further improvements of the interpolation formula have no effect. An adaptive 3D mesh[52] could significantly decrease the number of mesh points needed in the ATSUP method to achieve the precision required and thereby to reduce total computational time.

Finally, to simulate a finite resolution of the experimental detecting system, the convolution with a Gaussian function with the full width at half maximum (FWHM) of 4.2 mrad (i.e., 1.1 keV) is performed for all calculated HMP spectra. The FWHM selected corresponds to the resolution of the experimental apparatus used in Ref. 18. The final normalization of $\rho(p)$ distribution is chosen[9] so that the areas under calculated spectra are equal to $\lambda_c/\lambda_{tot}$ ($\lambda_c$ and $\lambda_{tot}$ are, respectively, the core and total annihilation rates). To make comparison with measurements meaningful, the areas under experimental spectra have to be normalized to unity.

There is an important question about how to choose the core states for the HMP calculations. Concerning Si it has been shown[9] that if one takes into account $1s$, $2s$, and $2p$ orbitals, a good agreement with experiment is achieved. Moreover, checking the energies of these states (using the atomic program[51]) leads to a maximum value of $-3.5$ Ry for $2p$ orbital, which can be considered as a well localized state (corresponding quantum-mechanical mean radius is 0.54 a.u.). In the case of oxygen we have decided to include $1s$ and $2s$ orbitals into core states.. The energy of the $2s$ orbital lies at about $-0.9$ Ry below the vacuum level and its mean radius is 1.15 a.u. We suppose that the $2s$ level is sufficiently low not to be significantly influenced if an O atom is placed in solids.

The positron lifetime, labeled further as $\tau$, is the inverse of the total annihilation rate, which can be determined using Eq. (3) where $n_-^{i,nl}$ is replaced by the total electron density $n_-$. Recently, Korhonen et al.[53] have shown that the positron lifetime depends on the supercell size when the supercell is not large enough. They have also suggested how to overcome this problem. The basic idea consists in determining the positron state for more **k** points in the Brillouin zone (not only in $\Gamma$ point) and making a **k**-space average of the positron density before the lifetime is calculated. We adopt this scheme in the present work.

## III. RESULTS AND DISCUSSION

### A. Basic positron properties

Calculated positron lifetimes corresponding to the bulk Si and defects studied are shown in Tables I (ATSUP results) and II (LMTO results) together with experimental data available. In the case of the LMTO method, we examine three selected defects only as calculations with large supercells are rather time expensive. The influence of the **k**-space integration[53] of the positron density on the positron lifetime (see Sec. II B) has been found to be quite small in our calculations. The maximum increase due to the integration occurs for the relaxed single vacancy and is 3 ps (ATSUP result). In the tables we also give the core annihilation rates, i.e., the sum of all $\lambda_{enh}^{i,nl}$'s over all atoms in the supercell and corresponding orbitals. Finally, we specify the positron binding energies to defects (calculated as the difference between the positron levels in the perfect and defected system).

We first discuss the LMTO calculations. We have found that the choice of the LMTO basis for positrons is important when calculating the positron properties for defects. This becomes clear if one inspects differences between the results obtained with the $s$ basis only and with the $s$, $p$, $d$ basis in Table II. The lifetimes are systematically higher when calculated with $s$ basis only. This is quite surprising as it is usually assumed that the positron wave function has a predominant $s$ character and adding further types of orbitals into basis should not have any significant influence. The origin of the effect noted above can be traced back to the different distri-

TABLE II. Comparison of results obtained using the BN and GGA computational schemes. Positron lifetimes ($\tau$), core annihilation rates ($\lambda_c$), and binding energies ($E_b$) are calculated using the LMTO method. Numbers in parentheses in the column $\lambda_c$ give the relative core annihilation rate, i.e., $\lambda_c/\lambda_{tot}$ (in %).

| System | Basis | LMTO-BN | | | LMTO-GGA | | |
|---|---|---|---|---|---|---|---|
| | | $\tau$ (ps) | $\lambda_c$ (ns$^{-1}$) (%) | $E_b$ (eV) | $\tau$ (ps) | $\lambda_c$ (ns$^{-1}$) (%) | $E_b$ (eV) |
| bulk | $spd$ | 220 | 0.161 (3.5) | | 211 | 0.108 (2.3) | |
| | $s$ | 217 | 0.170 (3.7) | | 209 | 0.114 (2.4) | |
| $V$ ideal | $spd$ | 258 | 0.091 (2.3) | 0.65 | 246 | 0.060 (1.5) | 0.69 |
| | $s$ | 274 | 0.073 (2.0) | 0.91 | 262 | 0.047 (1.2) | 0.97 |
| $V_2$ ideal | $spd$ | 299 | 0.045 (1.3) | 1.71 | 287 | 0.030 (0.9) | 1.74 |
| | $s$ | 313 | 0.039 (1.2) | 1.83 | 301 | 0.025 (0.8) | 1.89 |
| $V_2O$ relaxed | $spd$ | 286 | 0.077 (2.2) | 1.03 | 274 | 0.053 (1.5) | 1.10 |
| | $s$ | 306 | 0.063 (1.9) | 1.20 | 293 | 0.043 (1.3) | 1.29 |

butions of a positron among spheres in the supercell when using different bases. We have also examined the partial orbital occupancies of positrons in atomic (and empty) spheres for the $V_2O$ defect finding the $s$ occupancies to be in the range 70–100 % of the total ones ($d$ contributions being up to 5%). Henceforth, here we will consider the results obtained with the $s$, $p$, $d$ basis only.

Further we compare LMTO and ATSUP results. We can see a fair agreement in lifetime values calculated with the BN scheme. Concerning the GGA results the lifetimes for both $V_2$ (ideal) and $V_2O$ defects are considerably higher when calculated using the ATSUP method. A possible explanation is that the GGA enhancement factor is more sensitive to the shape of electron density (due to a factor that depends on the gradient of the electron density; see Ref. 29) and thereby to the self-consistency, i.e., to the charge transfer. Core annihilation rates depend more on details of positron density expansion around nuclei and therefore the differences between the ATSUP and LMTO results are slightly larger than in the lifetime case. The charge redistribution due to the self-consistency causes a deeper positron potential in the interstitial region (as the electron density increases here in comparison with the superimposed atomic density), which also results in higher binding energies. Nevertheless, there are a little bit larger deviations for the $V_2O$ defect from the trends found (for core annihilation rate and binding energy), which will be explained in the next section.

The comparison of BN and GGA results represents the next interesting point. The GGA enhancement factor and positron potential have been introduced very recently and they have to be tested carefully even if the treatment of core states is improved[29] considerably with respect to the BN one, which is manifested in apparently lower calculated values of the core annihilation rates in GGA scheme than in the BN one (see Tables I and II). Furthermore, we can see clearly that the GGA lifetimes are systematically below their BN counterparts. The only exceptions are $V_2$ and $V_2O$ defects (ATSUP case), already discussed above. If we look at calculated and measured bulk positron lifetimes, we can see that the GGA lifetimes slightly underestimate the experiment, but the BN bulk values agree well with the experimental one, which is known with a very good precision. Clearly, one comparison only is not sufficient to allow us to make a seri-

ous conclusion about the GGA scheme. In the case of imperfect systems, it is more difficult to assess the adequacy of an enhancement factor (and corresponding positron potential) when comparing calculated and measured quantities because of relaxations (and zero positron density approach used).

For a single vacancy the (inward) relaxations are rather big[22,33] and the positron-related relaxations are also large, but, according to recent work of Saito and Oshiyama,[22] they are in the opposite direction, so that the final positions of atoms lie slightly outwards with respect to the unrelaxed (ideal) defect. As we consider just the first relaxation effect, our calculated lifetimes for a single vacancy are in all cases much lower than the experimental value and value (279 ps) derived in Ref. 22. The divacancy is not so heavily influenced by relaxations[22,33] and our lifetime values are very close to the experimental ones even if those are rather scattered. To our knowledge, there are no experimental data available for $VO_n$ and $V_2O$ defects.

A concluding comment concerning the GGA scheme refers to negative binding energies for relaxed $V$ and $VO_3$ defects found with the ATSUP technique. They may indicate some shortcomings in the GGA positron correlation potential because plots of the positron density at defect sites and their neighborhood prove the positron localization. On the other hand, the negative binding energies are very small in magnitude and comparable with the numerical uncertainties of the technique used.

A few works[22,29,54–57] have appeared where positron-related properties of a single vacancy and divacancy in Si have been studied. Our calculated lifetimes and binding energies for these two defects treated within the ATSUP and LMTO methods agree well with corresponding values presented in Refs. 55 and 57. Bulk core annihilation rates (BN scheme) are well comparable with Ref. 56 as well. Our results are also in very good accordance with Ref. 29 where positron properties of bulk Si and ideal vacancy using both ATSUP-GGA and LMTO-GGA schemes have been examined.

At the end of this section we wish to discuss the possibilities of positron lifetime spectroscopy to differentiate among defects studied. According to Table I we have the following lifetimes (ATSUP-BN scheme): 218 (bulk), 222 ($VO_n$), 270 ($V$; experimental value), 302 ($V_2$), and 297
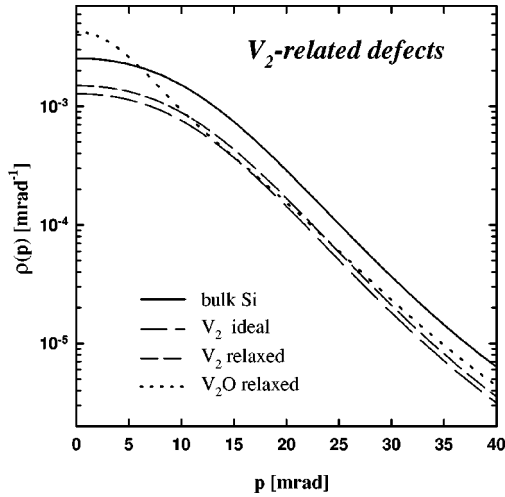
FIG. 1. HMP's of the MDAP for bulk Si as well as for the ideal and relaxed $V_2$ and $V_2O$ defects calculated within the ATSUP-BN scheme.

($V_2O$) ps. In practice one can distinguish lifetime components in a lifetime spectrum that differs more than 50 ps (at the 250-ps level). This shows significant limitations of PLS in the case of vacancylike defects in Si.

### B. Momentum distribution

In Fig. 1 we show HMP's of the MDAP for the bulk Si, ideal and relaxed $V_2$ defect, and for $V_2O$ complex calculated within the ATSUP-BN scheme. The curve for bulk Si agrees very well with calculations of Alatalo *et al.*[9] The curves for both $V_2$ cases lie well below the bulk one as expected, the curve for the relaxed defect being closer to bulk. However, the $V_2O$ dependence is above the bulk curve for small values of momentum but decreases faster with increasing $p$ so that it is again below the bulk curve for $p \gtrsim 6$ mrad.

In the following we will rather show the ratios of type $\rho^{\text{defect}}(p)/\rho^{\text{bulk}}(p)$, which visualize better differences among shapes and magnitudes of HMP curves.[12]

The HMP ratio curves obtained with the ATSUP method and GGA enhancement and positron potential for $V$- and $V_2$-related defects are given in Figs. 2(a) and 2(b), respectively. One can see an appreciable difference between the

ideal and relaxed single vacancy. The latter curve approaches a line with ratio equal to 1 (i.e., to the bulk curve) and we can expect that the curve would be further changed by considering an additional relaxation caused by the presence of a positron. In the case of the $V_2$ defect, the relaxations play a less important role and HMP curves for the ideal and relaxed defect are much closer, which is in accordance with discussion in Sec. III A. The curves corresponding to oxygen-related defects have qualitatively different shapes. This originates from the $2s$ core orbitals of the O atom, which are rather spatially extended (see also below). The shapes and relative positions of ratio curves shown in Figs. 2(a) and 2(b) suggest the idea that all defects are well distinguishable with the exception of the group of $VO_n$ defects. Ratio HMP curves of these defects differ considerably from other types of defects but not inside this group.

The same ratio curves calculated using the ATSUP-BN scheme have been presented in our previous paper [Figs. 1(a) and 1(b) in Ref. 18]. It is worth mentioning that even if there are differences between magnitudes of HMP curves obtained within the BN and GGA schemes due to appreciably lower core annihilation rates in the GGA case, the ratio curves are very similar. For some curves obtained with the ATSUP-BN scheme there is a slight shift to lower values in comparison with Fig. 2.

Calculating the HMP's of the MDAP turned out to be more intricate when using the LMTO method. Calculated ratio curves for selected defects (ideal $V$, ideal $V_2$, and $V_2O$) are shown in Fig. 3. The GGA scheme is applied in all these calculations. There is an apparent shift down of HMP ratio curves for all cases studied with respect to the curves calculated by means of the ATSUP method. This can be understood if we inspect relative core annihilation rates (i.e., $\lambda_c/\lambda_{\text{tot}}$ ratios; see Sec. II B) in Table II and compare them with corresponding values in Table I. Namely, the $\lambda_c/\lambda_{\text{tot}}$ ratio is higher for the bulk Si and lower for defects examined using the LMTO method.

In addition, the shape of ratio curves calculated within the LMTO-BN scheme is nonnegligibly changed in comparison with the ATSUP-GGA calculations. The most pronounced change occurs for the $V_2O$ defect. We have already mentioned differences between the ATSUP and LMTO calculations for this defect (see Sec. III A). Thus, $\lambda_c$ is reduced
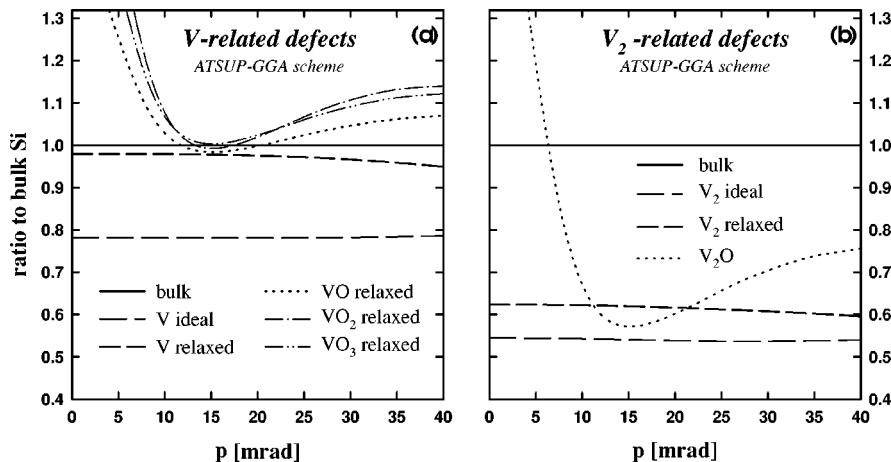


FIG. 2. Ratio HMP curves for (a) vacancy- (b) divacancy-related defects calculated within the ATSUP-GGA scheme.
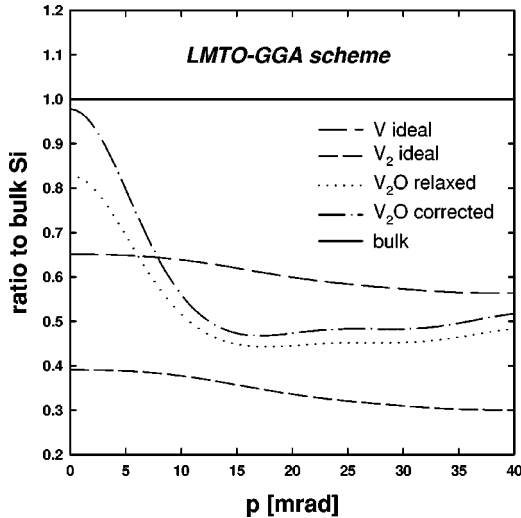
FIG. 3. Ratio HMP curves for unrelaxed V and $V_2$ defects, and divacancy-oxygen complex obtained using the LMTO-GGA scheme.

from 0.067 ns$^{-1}$ (ATSUP-GGA) to 0.053 ns$^{-1}$ (LMTO-GGA). A detailed inspection of partial annihilation rates ($\lambda_{GGA}^{i,nl}$) unveils that oxygen $2s$ electrons are mainly responsible for such a big reduction. Corresponding O $2s^2$ rates (state enhancement factors) are 0.035 ns$^{-1}$ (2.48) and 0.027 ns$^{-1}$ (1.92) for the ATSUP-GGA and LMTO-GGA scheme, respectively.

A closer look at the geometry of the $V_2O$ defect[5] shows that there is a Si-O-Si "bridge," next to divacancy, with very short distances (about 3.3 a.u.) between O and Si atoms. This means that the radii of corresponding atomic spheres of Si and O in the supercell describing the $V_2O$ defect have to be rather small to keep their overlaps within reasonable limits.[25] We have chosen radii 2.03 and 1.81 a.u. for two Si atoms and an O one, respectively, which leads to an Si-O overlap of 17%. For comparison, the radius 2.53 a.u. of Si atomic spheres (and empty spheres) is used in the bulk Si. We can conclude that the calculation of the partial annihilation rate for the oxygen $2s$ orbital, which is spatially more extended than Si core orbitals (see Sec. II B), is not precise enough due to a small radius of the O atomic sphere.

One could perhaps increase the size of the O atomic sphere, decreasing simultaneously the radii of Si spheres involved. But this process has naturally certain limits and it is not clear if the O $2s$ core annihilation rate would improve considerably. Instead we recalculate the HMP curve for the $V_2O$ defect using the enhancement factor and partial annihilation rate of the O $2s$ state taken from the ATSUP-GGA calculation. The resulting ratio curve is also plotted in Fig. 3 (dash-dotted curve). Now there is a slightly better agreement with the corresponding curve in Fig. 2(b). We should note, however, some tendency to oscillations in both $V_2O$ ratio curves. This effect probably stems from the inadequate continuation of the positron wave function beyond the atomic sphere radius (see Sec. II B) in the case when the radius is too small. Furthermore, it is probable that the positron density in the interstitial space is not well described by empty spheres around the $V_2O$ defect as can be deduced from a too low positron binding energy to the defect (see Table II and discussion in Sec. III A).

We do not show the ratio curves calculated within the BN scheme as they are very similar to those presented in Fig. 3. Moreover, the correction described above affects the HMP ratio curve of the $V_2O$ complex analogously.

At the end, we briefly resume experimental HMP data concerning oxygen-related defects in Si. In the work of Szapala et al.[12] no difference between the HMP's of Si ion irradiated Cz and FZ Si samples has been found. According to our calculations the spectrum of self-implanted Si shown in Ref. 12 does not correspond to the divacancy (or bulk + divacancy mixture) but rather to a $V_2$ and $V_2O$ mixture, though it is difficult to imagine that $V_2O$ defects are created in FZ Si samples in a higher concentration. On the contrary, our HMP measurements[18] have exhibited a clear distinction between FZ and Cz electron irradiated samples, which has allowed a rough identification of existing defects (see Ref. 18 for details).

In the work of Kruseman et al.,[15] O ion implanted Cz Si wafers have been studied. The authors have examined the changes of the HMP ratio curves with respect to the irradiation dose and annealing temperature. They suppose that large $V_mO_n$ clusters are created in implanted wafers upon annealing. Even if we have calculated the HMP ratio curves for $V_2O$ and $VO_n$ complexes only, the presence of larger $V_mO_n$ clusters in the curves shown in Ref. 15 seems to be indicated by the characteristic minima of these curves at about 20 mrad (see Figs. 2 and 3). Finally, Knights et al.[16] have also investigated Cz Si samples implanted by oxygen ions. Measured HMP ratio curves shown there have a minimum at roughly the same position as in Ref. 15. However, a further comparison of these two works is not straightforward as the normalization procedures of measured spectra differ.

## IV. CONCLUSIONS

We have calculated positron lifetimes, core annihilation rates, positron binding energies, and high momentum parts of the momentum distribution of annihilation photons for the perfect and defected Si. The single vacancy, divacancy, three types of vacancy-oxygen complexes, and divacancy-oxygen complex have been examined. The effect of atomic relaxations on the calculated positron quantities has been found to be the most pronounced for the single vacancy. The charge redistribution due to the self-consistency of the electron structure (obtained using the LMTO technique) results in larger binding energies of positrons to defects in comparison with the case when the non-self-consistent ATSUP technique is used. On the contrary, positron lifetimes are influenced by the charge transfer slightly only and no systematic trend has been observed. Regarding the HMP's of the MDAP, the positions and shapes of the ratio HMP curves are changed appreciably when the LMTO-ASA technique is employed instead of the ATSUP one. It has to be mentioned, however, that we have encountered problems in finding appropriate space filling with atomic and empty spheres in the case of oxygen-related defects studied using the LMTO-ASA technique. This indicates the limited applicability of this method for some defects with complicated geometry.

Calculated HMP curves can essentially help in the identification of defects studied in measured Doppler broadened spectra of defected Si samples as we have demonstrated in

our previous work.[18] However, further experiments are necessary to unambiguously resolve all relevant defects present in our samples. From the theoretical point of view, it would be desirable to perform a study of positron-related relaxations in the case of $VO_n$ and $V_2O$ complexes because this effect could somewhat influence the shape and magnitude of HMP curves. Moreover, in very recent works[58,59] vacancy-interstitial pairs in Si are supposed to be frozen at low temperatures and, therefore, an investigation of these pairs is also needed to have some idea of the behavior of a positron trapped in such defects.

*Author to whom correspondence should be addressed. Electronic address: honzakr@mbox.cesnet.cz

[1] See, e.g., *Early Stages of Oxygen Precipitation in Silicon*, edited by R. Jones (Kluwer Academic Publishers, Dordrecht, 1996).

[2] J. W. Corbett and G. D. Watkins, Phys. Rev. **138**, 555 (1965).

[3] G. D. Watkins and J. W. Corbett, Phys. Rev. **138**, 543 (1965).

[4] C. A. Londos, N. V. Sarlis, and L. G. Fytros, in *Early Stages of Oxygen Precipitation in Silicon*, edited by R. Jones (Kluwer Academic Publishers, Dordrecht, 1996), p. 477.

[5] C. P. Ewels, R. Jones, and S. Öberg, Mater. Sci. Forum **196-201**, 1297 (1995); see also C. P. Ewels, Ph.D. thesis, Exeter, 1997.

[6] M.-A. Trauwaert, J. Vanhellemont, H. E. Maes, A.-M. Van Bavel, G. Langouche, and P. Clauws, Appl. Phys. Lett. **66**, 3056 (1995).

[7] *Positron Spectroscopy of Solids*, edited by A. Dupasquier and A. P. Mills, Jr. (IOS Press, Amsterdam, 1995).

[8] M. Alatalo, H. Kauppinen, K. Saarinen, M. J. Puska, J. Mäkinen, P. Hautojärvi, and R. M. Nieminen, Phys. Rev. B **51**, 4176 (1995).

[9] M. Alatalo, B. Barbiellini, M. Hakala, H. Kauppinen, T. Korhonen, M. J. Puska, K. Saarinen, P. Hautojärvi, and R. M. Nieminen, Phys. Rev. B **54**, 2397 (1996).

[10] P. Asoka-Kumar, M. Alatalo, V. J. Ghosh, A. C. Kruseman, B. Nielsen, and K. G. Lynn, Phys. Rev. Lett. **77**, 2097 (1996).

[11] R. N. West, in *Positron Spectroscopy of Solids*, edited by A. Dupasquier and A. P. Mills, Jr. (IOS Press, Amsterdam, 1995), p. 75.

[12] S. Szapala, P. Asoka-Kumar, B. Nielsen, J. P. Peng, S. Hayakawa, K. G. Lynn, and H.-J. Gossmann, Phys. Rev. B **54**, 4722 (1996).

[13] U. Myler, R. D. Goldberg, A. P. Knights, D. W. Lawther, and P. J. Simpson, Appl. Phys. Lett. **69**, 3333 (1996).

[14] A. C. Kruseman, H. Schut, A. Van Veen, P. E. Mijnarends, M. Clement, and J. M. M. De Nijs, Appl. Surf. Sci. **116**, 192 (1997).

[15] A. C. Kruseman, H. Schut, M. Fujinami, and A. Van Veen, Mater. Sci. Forum **255-257**, 793 (1997).

[16] A. P. Knights, R. D. Goldberg, U. Myler, and P. J. Simpson, in *Early Stages of Oxygen Precipitation in Silicon*, edited by R. Jones (Kluwer Academic Publishers, Dordrecht, 1996), p. 411.

[17] M. Hakala, M. J. Puska, and R. M. Nieminen, Phys. Rev. B **57**, 7621 (1998).

[18] J. Kuriplach, T. Van Hoecke, B. Van Waeyenberge, C. Dauwe, D. Segers, N. Balcaen, A. L. Morales, M.-A. Trauwaert, J. Van-

hellemont, and M. Šob, Mater. Sci. Forum **255-257**, 605 (1997).

[19] M. J. Puska and R. M. Nieminen, J. Phys. F **13**, 333 (1983).

[20] L. Gilgien, G. Galli, F. Gygi, and R. Car, Phys. Rev. Lett. **72**, 3214 (1994).

[21] M. J. Puska, A. P. Seitsonen, and R. M. Nieminen, Phys. Rev. B **52**, 10 947 (1995).

[22] M. Saito and A. Oshiyama, Phys. Rev. B **53**, 7810 (1996).

[23] M. J. Puska and R. M. Nieminen, Rev. Mod. Phys. **66**, 841 (1994).

[24] R. M. Nieminen, in *Positron Spectroscopy of Solids*, edited by A. Dupasquier and A. P. Mills, Jr. (IOS Press, Amsterdam, 1995), p. 443.

[25] O. K. Andersen, O. Jepsen, and M. Šob, in *Electronic Band Structure and Its Applications*, edited by M. Yussouff (Springer Verlag, Heidelberg, 1987), p. 1.

[26] J. Arponen and E. Pajanne, Ann. Phys. (N.Y.) **121**, 343 (1979).

[27] E. Boroński and R. M. Nieminen, Phys. Rev. B **34**, 3820 (1986).

[28] M. J. Puska, S. Mäkinen, M. Manninen, and R. M. Nieminen, Phys. Rev. B **39**, 7666 (1989).

[29] B. Barbiellini, M. J. Puska, T. Torsti, and R. M. Nieminen, Phys. Rev. B **51**, 7341 (1995); B. Barbiellini, M. J. Puska, T. Korhonen, A. Harju, T. Torsti, and R. M. Nieminen, *ibid.* **53**, 16 201 (1996).

[30] D. J. Chadi, Phys. Rev. B **41**, 10 595 (1990).

[31] C. Z. Wang, C. T. Chan, and K. M. Ho, Phys. Rev. Lett. **66**, 189 (1991).

[32] E. G. Song, E. Kim, Y. H. Lee, and Y. G. Hwang, Phys. Rev. B **48**, 1486 (1993).

[33] H. Seong and L. J. Lewis, Phys. Rev. B **53**, 9791 (1996).

[34] J. L. Hastings, S. K. Estreicher, and P. A. Fedders, Phys. Rev. B **56**, 10 215 (1997).

[35] This choice is compatible with Ref. 5. In Ref. 33 a slightly different lattice constant is used.

[36] P. A. Sterne and J. H. Kaiser, Phys. Rev. B **43**, 13 892 (1991).

[37] M. Šob, in *Proceedings of the 10th Annual International Symposium on Electronic Structure of Metals and Alloys, Gaussig, Germany*, edited by P. Ziesche (Dresdener Seminar für Theoretische Physik, Dresden, 1980), p. 106.

[38] M. Šob, J. Phys. F **12**, 571 (1982).

[39] J. Svoboda and M. Šob, Philos. Mag. B **48**, 523 (1983).

[40] A. K. Singh, A. A. Manuel, T. Jarlborg, Y. Mathys, E. Walker, and M. Peter, Helv. Phys. Acta **59**, 410 (1985).

[41] P. Genoud, A. K. Singh, A. A. Manuel, T. Jarlborg, E. Walker, M. Peter, and M. Weller, J. Phys. F **18**, 1933 (1988).

[42] M. Matsumoto and S. Wakoh, J. Phys. Soc. Jpn. **56**, 3566 (1987).

[43] M. Matsumoto and S. Wakoh, Physica B **149**, 57 (1988).

[44] M. Šob, Solid State Commun. **53**, 249 (1985).

[45] M. Šob, Solid State Commun. **53**, 255 (1985).

[46] S. Daniuk, G. Kontrym-Sznajd, J. Majsnerowski, M. Šob, and H. Stachowiak, J. Phys.: Condens. Matter **1**, 6321 (1989).

[47] S. Daniuk, M. Šob, and A. Rubaszek, Phys. Rev. B **43**, 2580 (1991).

[48] R. Jastrow, Phys. Rev. **98**, 1479 (1955).

[49] B. Barbiellini, M. Hakala, M. J. Puska, R. M. Nieminen, and A. A. Manuel, Phys. Rev. B **56**, 7136 (1997).

[50] We have employed a symbolic manipulation software to derive this 3D-interpolation formula.

[51] J. P. Desclaux, Comput. Phys. Commun. **1**, 216 (1969); J. P. Desclaux, *ibid.* **19**, 31 (1975).

[52] E. L. Briggs, D. J. Sullivan, and J. Bernholc, Phys. Rev. B **54**, 14 362 (1996).

[53] T. Korhonen, M. J. Puska, and R. M. Nieminen, Phys. Rev. B **54**, 15 016 (1996).

[54] M. J. Puska, O. Jepsen, O. Gunnarson, and R. M. Nieminen, Phys. Rev. B **34**, 2695 (1986).

[55] M. J. Puska and C. Corbel, Phys. Rev. B **38**, 9874 (1988).

[56] M. J. Puska, J. Phys.: Condens. Matter **3**, 3455 (1991).

[57] M. J. Puska, Mater. Sci. Forum **105-110**, 419 (1992).

[58] M. Tang, L. Colombo, J. Zhu, and T. Diaz de la Rubia, Phys. Rev. B **55**, 14 279 (1997).

[59] H. Zillgen and P. Ehrhart, Nucl. Instrum. Methods Phys. Res. B **127**, 27 (1997).